Gelatin-genipin based biomaterials for skeletal muscle tissue engineering

Francesca Gattazzo, PhD[a,b], Carmelo De Maria, PhD[b], Alessandro Rimessi, PhD[c], Silvia Donà[a], Paola Braghetta, PhD[a], Paolo Pinton, PhD[c], Giovanni Vozzi, PhD[b*], Paolo Bonaldo, PhD[a,d*]

[a] Department of Molecular Medicine, University of Padova, Padova, 35131, Italy.

[b] Research Center "E. Piaggio," University of Pisa, Pisa, 56122, Italy.

[c] Department of Morphology, Surgery and Experimental Medicine, University of Ferrara, Ferrara, 44121, Italy.

[d] CRIBI Biotechnology Center, University of Padova, Padova, 35131, Italy

*** Correspondence:** Paolo Bonaldo, Department of Molecular Medicine, University of Padova, Via U. Bassi 58/B, I-35131 Padova, Italy. e-mail: bonaldo@bio.unipd.it; Giovanni Vozzi, Research Center "E. Piaggio," University of Pisa, Largo Lucio Lazzarino 1, Pisa 56122, Italy. e-mail: g.vozzi@ing.unipi.it

Keywords: Gelatin; Genipin; Skeletal muscle; Tissue engineering; Muscle regeneration.

Skeletal muscle engineering aims at tissue reconstruction to replace muscle loss following traumatic injury or in congenital muscle defects. Skeletal muscle can be engineered by using biodegradable and biocompatible scaffolds that favor myogenic cell adhesion and subsequent tissue organization. In the present study, we characterized scaffolds made of gelatin cross-linked with genipin, a natural derived cross-linking agent with low cytotoxicity and high biocompatibility, for tissue engineering of skeletal muscle. We generated gelatin-genipin hydrogel with a stiffness of 12 kPa to reproduce the mechanical properties characteristic of skeletal muscle and we show that their surface can be topographically patterned through soft-lithography in order to drive myogenic cells differentiation and unidirectional orientation. Furthermore, we demonstrate that these biomaterials can be successfully implanted *in vivo* under dorsal mouse skin, showing good biocompatibility properties and slow biodegradation rate. We also demonstrate that the grafting of this biomaterial in partially ablated tibialis anterior muscle does not impair muscle regeneration, supporting future applications of gelatin-genipin biomaterials in the field of skeletal muscle tissue repair.

1. Introduction

Skeletal muscle is a highly complex organ, mainly characterized by bundles of aligned multinucleated myofibers, necessary for the generation of contraction and strength. One distinct feature of this tissue is its innate capability to regenerate after damage in a highly orchestrated manner, a feature that is largely provided by a specific population of stem cells, named satellite cells (1). This regenerative capability is impaired under a number of pathological conditions, such as traumatic injury or inherited muscle diseases, as well as in aging-related sarcopenia.

Muscle tissue engineering approaches aim at repairing or regenerating skeletal muscle by making use of myogenic cells, scaffolds, bioactive molecules or combination thereof. Towards this aim, *in vitro* tissue engineering approaches make use of cells and biomaterials for developing a mature and contractile-engineered muscle construct. *In vivo* strategies rely upon the transplantation of myogenic cells in skeletal muscle, either alone or in combination with scaffolds that recreate the local microenvironment and allow the integration of cells in the host tissue or promote novel tissue formation. *In situ* engineering approaches use biomaterials to release multiple bioactive and chemotactic signals and display surface cues in order to activate, recruit and reorganize host cell populations (2). In each of these strategies, high importance is given to the realization and optimization of the scaffold. Indeed, optimal scaffolds should *i)* support myogenic cell growth and differentiation; *ii)* behave as a muscle stem cell niche, by mimicking the native environment to which myogenic cells are exposed (3); *iii)* be biocompatible, in order to reduce the immune response in the host muscle; *iv)* be biodegradable, to gradually allow the substitution of the scaffold by the newly formed muscle (4). Furthermore, several technologies have been applied to control the orientation of cells and mimic the unidirectional alignment of myotubes, including the fabrication of parallel linear microgrooves (5–7), the micro-patterning of the surface with tracks of extracellular matrix molecules (8–10), the application of an uniaxial strain in deformable

membranes on which cells are grown (11), the application of electrical excitation (12), or the use of bioreactors (13).

Here we propose the use of hydrogels composed of gelatin cross-linked with genipin (GP) for tissue engineering of skeletal muscle. Gelatin, which is essentially denatured collagen, has a myriad of uses in the food, pharmaceutical and cosmetic industries thanks to its biocompatibility, but shows poor mechanical properties and thermal instability. GP is a naturally occurring and low-cytotoxic crossing agent, which is derived from its parent compound geniposide isolated from the fruits of *Gardenia jasminoides Ellis*. GP is able to form stable products with resistance against enzymatic degradation, and is known for its anti-inflammatory and fibrolytic properties (14–16). GP has been used in the preparation of cross-linked gelatin films and hydrogels (17,18), for drug delivery purposes (19,20) and for regenerative applications, including wound dressings (21), chondrogenic differentiation (22), nerve guiding conduits (23,24), cartilage scaffolds (25), bone scaffolds (26,27) and arteriogenesis (28). To our knowledge, gelatin-GP biomaterials were not yet tested for myogenic cell culture or for skeletal muscle applications. Our results show for the first time that gelatin-GP biomaterials with mechanical properties resembling those reported for skeletal muscle support myogenic cell growth and differentiation, and also allow the unidirectional orientation of myotubes when their topology is properly micro-patterned. Moreover, our results demonstrate that this material display good biocompatibility and slow biodegradation rate after *in vivo* implantation. Grafting of acellular gelatin-GP scaffold in injured tibialis anterior (TA) muscle confirmed that the material is not detrimental for muscle regeneration, thus pointing at gelatin-GP scaffolds as useful biomaterials for skeletal muscle tissue engineering.

2. Materials and methods

Fabrication and characterization of scaffold

Genipin (GP) (Challenge Bioproducts Co., Ltd) was added at 0.2 % (w/v) to a solution of gelatin (Sigma) in PBS at different concentrations ranging from 1% to 10% (w/v). Each mixture was kept at 37 °C under moderate stirring until polymerization was started, as indicated by turning into blue color. The polymer solution is casted in the mold and the samples so obtained were left at room temperature for 48 hr until polymerization is stopped. After this time, mechanical properties were measured by compressive load-unload cycles with Zwick/Roell Z005 device with the following settings parameters: 0.01 mm/s, strain rate; 10% strain, end of loading phase; no load, end of load-unload cycle. The Young's modulus of each sample was evaluated from the slope of the initial linear portion of the stress-strain curve. At least ten specimens for condition were tested.

Replica Molding

A mask with parallel strips of 50 μm, 100 μm and 200 μm width and 100 μm strip separation was generated. Photoresist (NANOTM SU-8, Microchem) was spun coated onto 10 mm x10 mm wafers, producing a 40-μm thick layer, and the pattern was transferred to the silicon wafer (University Wafers) by exposing to UV light the photoresist through the mask. Then the wafer was developed using MF-319 developer (Microchem) and post-baked at 115 °C for 90 sec. PDMS solution was prepared (Sylgard 184, Dow Corning), casted onto the topographically patterned photoresist and cured overnight at 70 °C to allow PDMS stamp polymerization. After the fabrication process, the PDMS membrane was removed from the wafer, coated with 0.2% (w/v) pluronic (Invitrogen) to prevent hydrogel adhesion, and covered with 12 ml of gelatin-GP solution. Hydrogel was dried at RT and gently detached from PDMS mold, thus obtaining parallel strips of 50 μm, 100 m and 200 μm width and 100 μm strip separation, and 40 μm thick, cut into pieces (3 mm x 3 mm), rehydrated in PBS and sterilized for cell seeding. For SEM analysis scaffolds were dried, dehydrated in graded alcohol solution, critical point dried, sputter-coated with gold, and

analyzed in a Philips XL 20 scanning electron microscope. For cell seeding, samples were rinsed in PBS to remove GP residues, kept in 70% ethanol overnight, washed with PBS, sterilized under UV light and kept in PBS until use. Metallic rings were used to anchor the biomaterial to the well plate during the seeding and culture procedure.

Cell culture

C2C12 cell line (CRL-1722, ATCC) was cultured and differentiated at 37 °C and 5% CO_2. Cells were expanded in growth medium (DMEM supplemented with 10% fetal bovine serum, 200 mM L-glutamine and 1% penicillin–streptomycin) in T-75 flasks and split 1:3 when cultures reached 80% confluence. Glass cover slips were coated with gelatin 0,1% in PBS and used as control for each experiment. For proliferation analysis, cells were seeded as a single cell suspension at a density of 10 x 10^4 cells cm^{-2} onto 13 kPa flat gelatin-GP substrate or glass control and kept in culture for 24 hr. For differentiation studies, cells were seeded as a single cell suspension at a density of 35 x 10^4 cells cm^{-2} on the flat gelatin-GP substrate and glass control and as droplet on micro-patterned gelatin-GP substrates, and cultured for 1 day in growth medium. Cells were then cultured in differentiation medium (DMEM supplemented with 2% horse serum, 200 mM L-glutamine and 1% penicillin–streptomycin) for 7 days to induce myotube formation. Medium was changed and freshly added every 2 days. For primary myoblast cultures, single muscle fibers were isolated from extensor digitorum longus (EDL) of 2-month-old wild-type mice. Freshly isolated satellite cells were stripped off the fibers by repeated passage through a 18-gauge needle (29). Debris were then seeded onto a matrigel-coated 35-mm-dish in F10 medium supplemented with 20% fetal bovine serum, 25 ng/ml bFGF and 1% penicillin/streptomycin (all from Invitrogen). When satellite cells left their parental myofibers and started proliferating, they were trypsinized and expanded in matrigel-coated dishes. SC-derived myoblasts were seeded at 15 x 10^4 cells cm^{-2} on micro-patterned gelatin-GP substrate and cultured in F10 medium supplemented with 20% fetal bovine serum and 1% penicillin/streptomycin. After one day in proliferation medium, cells were cultured in differentiation media for 7 days as described above.

Immunofluorescence staining on cells and image analysis

Cells were fixed for 5 min with 4% paraformaldehyde, permeabilized for 10 min in the presence of 0.1% Triton X-100 in PBS, and incubated for 30 min with a blocking solution containing 10% goat serum (Sigma) in PBS. Cells were incubated overnight at 4° C with anti-rabbit Ki-67 (Abcam), anti-rabbit α-actin (Sigma) and anti-mouse myosin heavy chain (MyHC; MF20, Developmental Hybridoma Bank). Slides were incubated for one hour with the following secondary antibodies from Jackson Immunoresearch: anti-rabbit CY2 (1:500) or anti-rabbit CY3 (1:1000), anti-mouse CY2 (1:500) or anti-mouse 405 (1:200) diluted in 5% goat serum in PBS solution. Nuclei were stained with Hoechst 33258 (Sigma) or propidium iodide. Slides were mounted in 80% glycerol-PBS and analyzed by fluorescence microscope. The analysis of cell proliferation was performed by calculating the number of nuclei positive for Ki67 on the number of total nuclei, based on images taken at 20x magnification. For differentiation analysis only MyHC-positive cells with two o more nuclei were rated as myotubes. The fusion index was calculated as the ratio of the number of nuclei in myotubes to the number of total nuclei, based on images taken at 20x magnification. Myotube alignment was calculated as the angle between the long axis of a myotube and mean orientation axis of the structure (defined as 0°). Myotube length and width were measured using built-in functions of ImageJ software from 10x magnification. The 3-D rendering of the micro-patterned construct was performed using the ImageJ 3-D View plugin.

Fura-2/AM measurements

The cytosolic free Ca^{2+} concentration ($[Ca^{2+}]_c$) was evaluated using the fluorescent Ca^{2+} indicator Fura-2 acetoxymethyl ester (Fura-2/AM; Molecular Probes). Briefly, cells were incubated in medium supplemented with 2.5 μM Fura-2/AM for 30 min, washed with Krebs-Ringer buffer to remove the extracellular probe, supplied with preheated Krebs-Ringer buffer (supplemented with 1 mM $CaCl_2$), and placed in a thermostated (37 °C) incubation chamber on an Olympus Xcellence system (Olympus Corporation). Fluorescence was measured every 100 millisec with the excitation wavelength alternating between 340 and 380 nm and the emission fluorescence

being recorded at 510 nm. At the end of the experiment, a region free of cells was selected, and one averaged background frame was collected at each excitation wavelength for background correction. The $[Ca^{2+}]_c$ was calculated by the ratio method using the equation: $[Ca^{2+}]_c = Kd\ (R - R_{min}) / (R - R_{max})$ x Sf2 / Sf1 where Kd is dissociation constant of Fura-2/AM for (Ca^{2+}) taken as 240 nM at 37 °C, R is ratio of fluorescence for Fura-2/AM at the two excitation wavelengths, F340/F380, R_{max} is ratio of fluorescence in the presence of excess of calcium obtained by lysing the cells with 10 µM ionomycin (Sigma Aldrich), R_{min} is ratio of fluorescence in the presence of minimal calcium obtained by lysing the cells and then chelating all the Ca^{2+} with 0.5 M EGTA, Sf2 is fluorescence of Ca^{2+} free form of Fura-2/AM at 380nm excitation wavelength and Sf1 is fluorescence of Ca^{2+} bound form of Fura-2/AM at 380 nm excitation wavelength.

Mice

In vivo experiments were performed in wild-type mice of the inbred C57BL/6NCrl strain. Mice were housed in individual cages in an environmentally controlled room (23 °C, 12 hr light/12 hr dark cycle) and provided food and water *ad libitum*. Mouse procedures were approved by the Ethics Committee of the University of Padova and authorized by the Italian Ministry of Health.

Biocompatibility of biomimetic structures

Four-month-old female C57BL/6NCrl animals were anesthetized with Avertin (Sigma-Aldrich), the back of the animals was shaved and the exposed skin was treated with povidone-iodine solution to create an aseptic environment at the surgical site. Then an incision of 1 cm in length was performed and sterile micro-patterned biomaterials (3 mm x 4 mm) were gently implanted subcutaneously in the back. After implantation, skin was closed using 6/0 Prolene sutures (Ethicon Inc.). Implants were removed upon sacrifice at 1 week, 3 weeks and 6 weeks after implantation.

Surgical implantation of scaffold in injured muscle

Four-month-old female C57BL/6NCrl were anesthetized using Avertin (Sigma-Aldrich), and ≈4 mg wedge of tissue was removed by longitudinal cutting from the core of TA muscles (30). Removed

tissue was weighted in order to assess the repeatability of the ablation. A micro-patterned structure was laid down on the ablation site, and skin was closed using 6/0 Prolene sutures (Ethicon Inc.). The controlateral forelimb received only tissue removal and surgical closure and was used as control.

Histological analysis

Isolated implants with surrounding tissue and TA muscles were frozen in cold isopentane in liquid nitrogen and kept at −80 °C until use. Cross-sections (10 μm thick) were processed with hematoxylin-eosin for body reaction evaluation or Azan-Mallory to identify fibrosis and to quantify capsule thicknesses around implants. Myofiber cross-sectional area was evaluated with the IM1000 software (Leica).

Immunofluorescence staining on tissue sections

Frozen TA sections (8 μm thick) were fixed and permeabilized for 10 min with methanol-acetone at –20 °C, washed in PBS, incubated for 30 min with a blocking solution containing 10% goat serum (Sigma) in PBS. The following primary antibodies were used: rat anti-CD68 (1:300, AbD Serotec); rat anti-CD45 (1:300, Bethyl); rat anti-ER- TR7 (1:300, Santa Cruz); rabbit anti-laminin (1:800; L9393, Sigma), rabbit anti-collagen IV (1:500, Millipore). After washing, samples were incubated for 1 hr at room temperature with the appropriate secondary antibody provided by Jackson Immunoresearch where not indicated. Secondary biotinylated anti-mouse antibody (1:1000) was revealed with Cy3 streptavidin (1:1500). Other secondary antibodies used were anti-rabbit IRIS5 (1:250, Cyanine Technologies); anti-rabbit CY2 (1:500); anti-rat Cy3 (1:300). Staining with antibody against mouse Pax7 (1:20; Developmental Studies Hybridoma Bank) was carried out as described (31). Nuclei were stained with Hoechst 33258 (Sigma). Slides were mounted in 80% glycerol-PBS and analyzed by fluorescence microscopy.

Statistical analysis

213 Statistical significance for two groups of data was determined by unequal variance Student's t test
214 for normally distributed data or by Mann-Whitney-Wilcoxon Test in R for data that were not
215 normally distributed. Statistical significance for multicomparison data was analyzed using the
216 Kruskal-Wallis one-way ANOVA test followed by Tukey's test using the Matlab Statistic Toolbox
217 (The MathWorks, USA). Data are expressed as mean ± standard error of the mean (s.e.m) in all
218 conditions. A *P* value of less than 0.05 was considered statistically significant.
219

3. Results

Gelatin-GP biomaterials sustain cell growth and myogenic differentiation

By making use of different concentration of gelatin dissolved in PBS (from 2% to 10% weight on total volume) together with a fixed non-toxic concentration of GP (0.2% of total final volume), we generated scaffolds with compressive Young modulus ranging from 2 kPa to 75 kPa, and based on prior publication, we selected the biomaterial corresponding to a concentration of 4% gelatin (Fig. 1A) to mimick the stiffness value in the physiological range of skeletal muscle (≈12 kPa;(32,33)). To test whether the selected biomaterial could allow myogenic differentiation, we seeded C2C12 myogenic cells at subconfluence and we differentiated the cells for 3 days and 7 days, using glass coverslips as a control. Immunofluorescence analysis for the late myogenic differentiation marker MyHC (Fig. 1B) and quantification of MyHC-positive myotubes (with more than 2 nuclei) revealed a significant increase in the number of myotubes grown on the biomaterial compared to glass control at both 3 and 7 days (Fig. 1C). The increased number of myotubes on the biomaterial was associated to a higher number of total nuclei compared to glass control (Fig. 1D). On the other hand, the fusion index, calculated as the number of nuclei incorporated in myotubes *vs* the total number of nuclei, was similar for the two conditions (Fig. 1E). Myotubes appeared more elongated and narrow when grown on the biomaterial compared to glass control (Fig. 1B, F). We found that the increase of total nuclei observed on the biomaterial compared to glass control was linked to a two-fold increase in the percentage of proliferating Ki67-positive cells, measured one day after seeding (Fig. G-I). These data indicate that gelatin-GP biomaterials with 13 kPa favor C2C12 proliferation and allow myogenic differentiation.

Micro-patterned gelatin-GP structures promote the orientation and elongation of C2C12 myotubes

In order to mimic the organization of skeletal muscle into arranged and aligned myotubes, and based on the fact that the diameter of adult muscle fiber ranges from 10 μm to 100 μm (34), we

modified the whole surface of the 13 kPa gelatin-GP material by generating repetitive parallel strips of 50 μm, 100 μm or 200 μm width, 40 μm height, separated by a deeper 100 μm-wide groove (Fig. 2A). When seeded on the micro-patterned structures C2C12 cells adhered both to the groove and the strip spacing, and appeared to be oriented in the micro-patterning direction since the first day in culture (data not shown). After 7 days of culture in differentiation medium, 90% of MyHC myotubes were unidirectionally aligned on micro-patterned structure, at difference from cultures maintained on a non-patterned flat substrate with the same stiffness (Fig. 2B,C). The micro-patterned topology was effective in increasing both the elongation (Fig. 2D) and the maturity of myotubes, as indicated by the increased nuclear index (i.e., the mean number of nuclei per myotubes) (35) (Fig. 2E) and the higher fusion index (Fig. 2F). Differentiated C2C12 myotubes did not spontaneously contract in culture, neither on glass nor on the biomaterial, and only few striations were noticed on the micro-patterned biomaterial but not on glass control (Supplementary Fig. S1). To assess the functionality of myotubes in our culture system, we measured cytosolic free Ca^{2+} concentrations by making use of Fura-2/AM calcium-sensitive dye. Generation of Ca^{2+} fluxes demonstrated that myotubes grown on the micro-patterned biomaterial were responsive to carbachol administration (Fig. 2G), thus providing a proof of concept of the feasibility of the use of micro-patterned gelatin-GP biomaterials for electrophysiological studies. Altogether, these data indicate that micro-patterned gelatin-GP biomaterials are effective in guiding myotube orientation and promoting myotube differentiation.

Strip spacing influences the alignment of C2C12 myotubes

We then evaluated the contribution of strip spacing on the alignment of myotubes. Matrix topography was found to elicit a substantial effect on myotube size and orientation (Fig. 3). Not only myotubes were aligned in the groove spacing, but they were also aligned on upper strips (Fig. 3A, B; Supplementary Fig. S2). The mean orientation degree was under 10° for each micro-construct width considered, and the best orientation was observed on 50 and 100-μm-wide spacing. Interestingly, the topology dimension appeared to be the driving force of alignment, since no

significant difference was observed between 100-μm-wide groove and 100-μm-wide spacing. No significant difference was found between 50- and 100-μm-wide strips, indicating that 100 μm may be the optimal size for a material with a fixed groove and strip spacing (Fig. 3C). On the wider strips with 200 μm width, myotubes were significantly less oriented when compared to the narrower strips and groove spacing, and myotubes appeared significantly shorter and larger when compared to 50- and 100-μm-wide strips (Fig. 3E, F), despite a similar nuclear index (Fig. 3D). No significant differences were observed in the length and width of myotubes cultured on 50- and 100-μm-wide strips (Fig. 3E, F).

Micro-patterned gelatin-GP structures promote the orientation of primary myotubes

To test the feasibility of the chosen gelatin-GP biomaterial in sustaining the culture of primary myoblasts, we isolated satellite cells from mouse EDL muscle and differentiated them into myoblasts that were then cultured on the micro-patterned structures. Primary myoblasts attached to gelatin-GP substrates without any coating, with a preference on the strip spacing compared to the groove spacing, and were able to differentiate on the substrates, as shown by immunofluorescence staining for MyHC at 7 days culture in differentiation medium (Fig. 4A). At this time point myotubes were aligned on each groove spacing, as shown by an orientation degree lower than 10°, but myotubes grown on 50 μm showed a better orientation when compared to 200-μm wide strips (Fig. 4B). Primary myotubes were less sensitive than C2C12 myotubes to the topology of the biomaterial, as no significant difference was observed in their nuclear index, as well as in myotube length and width, among 50, 100 and 200-μm wide strips (Fig, 4C-E). Notably, and at difference from C2C12-derived myotubes, primary myotubes were capable to spontaneously contract on the biomaterial and higher magnification revealed the formation of sarcomeric structures (Fig. 4F; Supplementary Movie).

Gelatin-GP scaffolds are biocompatible *in vivo* and display a slow biodegradation rate

We then investigated the feasibility to use such materials not only for *in vitro* but also for *in*

296 *vivo* applications. Towards this aim we performed an incision (1 cm in length) in the dorsal skin of
297 wild-type mice and implanted subcutaneously a micro-patterned structure (0.3 cm x 0.5 cm). The
298 biocompatibility of the material was evaluated at 1 week, 3 and 6 weeks after implantation.
299 Macroscopic examination revealed the absence of any sign of edema or rash soon after the surgery
300 and at different time points after implantation, indicating that the material did not elicit rejection
301 responses. Interestingly, given its deep blue color, the structure could be easily identified under the
302 skin (Supplementary Fig. S3). Hematoxylin-eosin staining confirmed that the structure was still
303 present after 6 weeks from implantation, but its thickness appeared reduced and its internal porosity
304 increased (Fig. 5A, B). In addition, the surface appeared more irregular and undergoing a
305 degradation process (Fig. 5A), as indicated by a layer of mononucleated cells that persisted around
306 the structure for all the time points considered. Interestingly, at 7 days from implantation, some
307 mononucleated cells were adherent on the biomaterial surface both on the upper and lower sides,
308 whereas they began to appear in the more internal region of the substrate at 3 and 6 weeks from
309 implantation (Fig. 5A). Azan-Mallory staining showed a fibrotic capsule surrounding the
310 biomaterial, and morphometric analysis indicated that its thickness reached a peak 3 weeks after
311 implantation but was significantly reduced after 6 weeks (Fig. 5C, D). Immunofluorescence staining
312 for the main cell populations involved in the foreign body reaction indicated that the majority of
313 cell recruited in the site of implantation were macrophages (CD68-positive cells) and fibroblasts
314 (ER-TR7-positive cells), with some of those cells adherent onto the structure at 7 days from
315 implantation (Fig. 5E). Notably, their number increased at 3 and 6 weeks from implantation, and
316 those cells were found invading the structure and surrounding its degrading parts (Fig. 5E). These
317 findings reveal that the inflammatory resolution stage was ongoing, thus showing that micro-
318 patterned gelatin-GP structures are biocompatible and biodegradable, and indicating that the
319 degradation time and the re-absorbance of the fibrotic tissue capsule take more than 6 weeks.

320 **Gelatin-GP biomaterials do not impair skeletal muscle regeneration**

321 We next evaluated the feasibility of engrafting micro-patterned gelatin-GP structures in

murine TA muscle. To reproduce a condition in which biomaterial construct implantation is needed, such as muscle damage, we subjected TA muscle to a partial muscle ablation. Ablation of myofibers was chosen in order to stimulate muscle regeneration and at the same time generate an empty space that can be taken over by the biomaterial itself (Supplementary Fig. S4). Histological analysis revealed that the partial ablation of muscle fibers was efficient in inducing regeneration in a limited portion of the external region of TA, and that the cross-sectional area of regenerating centrally nucleated myofibers increased with time, with only a slight significant difference between control and grafted animals despite the inflammatory process and the presence of mononucleated cells in the latter (Fig. 6 A, B). To verify the identity of infiltrating cells surrounding and adhering to the surface of the biomaterial, we performed immunofluorescence for different regenerative and inflammatory markers. At 7 days after muscle damage, no Pax7-positive satellite cell was found adherent on the surface of the structure or in the more proximal region adjacent to the structure, indicating that the structure alone did not attract satellite cells, which were found associated with myofibers in both control and grafted TA (Fig. 6C). As observed in the dorsal skin implantation experiments, the majority of cells found in the proximity of the structure, at both 7 days and 1 month after damage, were CD68-positive macrophages and CD45-positive cells (Fig. 6D; Supplementary Fig. S5). CD45- and CD68-positive cells were already attached on the biomaterial surface at 7 days after implantation and their number increased at 1 month, where cells were also infiltrating inside the structure. These findings indicate that the degradation of the grafted structure was undergoing, but the degradation process is slow and takes more than 4 weeks.

4. Discussion

In this work, we investigated the use of biomaterials composed of gelatin cross-linked with GP for skeletal muscle tissue engineering applications and we tested their *in vitro* and *in vivo* biocompatibility. Our results show for the first time that besides their use for bone, nerve and cartilage repair and arteriogenesis (25,26,28,36), gelatin-GP biomaterials may found application also in the field of skeletal muscle regeneration, thanks to the possibility to modulate their mechanical properties and 3D architecture, and to their biocompatibility for myogenic cell culture.

One of the advantages of this material relies upon its tunable mechanical properties, leading to the generation of a broad range of stiffness values (from 2 to 75 kPa in our study), including those of skeletal muscle. Despite it was far from our interest, this observation points at gelatin-GP materials as potential scaffolds for the engineering of different tissues (37), and as suitable tool for investigating the biomechanical and biochemical effects of the extracellular matrix on cells (38). Concerning our interest, we selected gelatin-GP biomaterials with a stiffness value of 13 kPa for mimicking the elastic modulus previously published for skeletal muscle (32,33,39) and we observed an increased in the proliferation of C2C12 cells and the number of differentiated myotubes compared to glass control. This observation was in accordance with literature data showing that myogenic differentiation is promoted on a stiffness around 10-15 kPa (37) and with the observation that increased myoblast proliferation and differentiation can be observed with natural hydrogel composed of alginate with “myogenic” stiffness between 13 and 45 kPa (40). Together with the regulation of the mechanical properties, the realization of the anisotropic alignment of myotubes is an essential condition for mimicking the native skeletal muscle. The efficacy of this technology in driving myotube orientation at both nano- and micro-scale levels has been showed by various studies both for rodent and human myogenic cell (5,35,41–48), and confirmed by us with the use of graded gelatin-GP biomaterial with 50, 100 and 200 μm wide strips, separated by fixed 100 μm grooves of 40 μm height, not only with C2C12 cells but also with primary myoblasts. The effects

on the elongation and orientation of myotubes cultured on materials with strips of different width are triggered by a reorganization of the cytoskeleton in response to the cues provided by surface features. In general, when different spacing strip are analyzed, both C2C12 cells and mouse primary myoblasts exhibit greater alignment on substrates with smaller groove spacing (49–51). Similarly to strip width, it is known that grooves with a height more than 10 μm are responsible of a physical restriction of cells (48). Despite we did not characterize in detail some parameters, as the proliferation rate on the different wide-strips or the fusion index, the effect on orientation was clear and in accordance with other works evaluating the effect a similar range of dimension, from 50 to 500 um, on myogenic cells alignment and orientation (8,9,46,52,53). Our global analysis show that the patterning of the biomaterial promoted a higher rate of myotube maturation in terms of fusion index and nuclear index when compared to unpatterned substrates. However, at a difference from the previusoly cited works, C2C12 myotubes did not show good level of maturation, as shown by only slight appearance of striation, a result that may rely upon the selected batch of cells that did not show high degrees of maturation neither on the glass control. On the contrary, primary myotubes spontaneously contracted when cultured onto micro-patterned substrates. Although future work will be focused in enhancing the culture conditions, our present results provide a proof of concept of the feasibility of the use of micro-patterned gelatin-GP biomaterial to generate *in vitro* cultures of unidirectionally aligned contracting primary myotubes where electrophysiological studies can be performed. A recent publication refers to the use of micropatterned gelatin hydrogel for C2C12 allignement but makes use of a different cross-linker and smaller strip size but does not show any *in vivo* characterization (54). Despite this, this other work confirm the advantage of directly micromolding a natural hydrogel as gelatin compared to commonly used extracellular microcontact printed PDMS (9,54), in terms of efficiency of growing and orienting myotubes for long term cultures. Even if we did not analyzed our cells after 3 weeks in culture we could assume that our system may be as effective as theirs, and find application for muscle development and disease and chronic drug testing *in vitro.*

One of the potential drawbacks of GP is the generation of a blue colored structure that displays strong autofluorescence. Although on the one side this limits the use of immunofluorescence staining (55), on the other side it is extremely useful for the detection of the implanted biomaterial after *in vivo* grafting. In order to have a further characterization of the material for *in vivo* applications, we engrafted micro-patterned gelatin-GP structures either under dorsal skin or on injured TA muscle of non-immunodeficient mice. The choice of implanting the micro-patterned biomaterial, instead of the flat one, was due to the interest in assessing the features of a material capable to orient myoblasts, in the perspective to use it in the future with embedded myogenic cells. In our experimental setting, both skin and muscle grafting revealed that the acellular micro-patterned gelatin-GP material was well received, showing a biodegradability of over than 6 weeks. This result was consistent with the long biodegradation rate observed for gelatin-GP cross-linked materials as peripheral nerve guide conduit, either alone or embedded with adipose-derived stem cells (23,36). Although in those studies the mechanical properties of the material were not characterized, the authors reported that a 0.11-0.15 mm thick conduit was still present after 8 weeks, despite some signs of degradation at 6 weeks and a thin fibrotic capsule around the structure (36). It can be hypothesized that the long biodegradation rate of the implanted micro-patterned gelatin-GP biomaterial may be linked to its thickness (~200 μm), suggesting that this aspect may represent a critical parameter for tissue engineering applications. On the one side, for skeletal muscle application it would be desirable that the degradation rate of the implanted material last about 4-6 weeks, corresponding to the rate of new tissue formation (56,57), implying that the biomaterial thickness should be reduced. Neverthless, the biodegradation time of several natural biomaterials used for skeletal muscle application are variable, varying from up to 12 weeks for decellularized muscle matrix (58,59) or limited to 39 days for alginate gels (60), based on their different composition, cross-linking, dimension and internal porosity. On the other side, a long biodegradation should be desirable in the case of muscles necessary to sustain specific anatomical locations, such as the abdominal wall, or for the long-lasting release of drugs.

One of the main issues associated with protein-based scaffolds is immune rejection and the onset of a foreign body response (61) leading to many *in vivo* studies being carried out in immunodeficient animal models at a difference from our study. Our analysis revealed the presence of macrophages and inflammatory cells degrading the structure at 3 and 6 weeks after implantation, nevertheless our data indicate that the long permanence of the biomaterial alone did not interfere with muscle regeneration in our model of injury of the TA muscle. Further studies will be aimed at evaluating the timing of complete degradation of the material and of the fibrotic capsule, together with a more detailed analysis of the inflammatory response in terms of macrophages polarization. Persistent macrophage polarization into M1 is associated with fibrotic and scar tissue formation, whereas anti-inflammatory M2 macrophages are known to guide the resolution of the inflammatory stage and also to stimulate the proliferation and differentiation of satellite cells toward the formation of new fibers (62,63). Given the naturally derived origin of our biomaterial, it would be worth to deeply investigate whether gelatin-GP scaffolds may promote the switch of macrophages from an M1 to an M2 phenotype as it was observed during the degradation of decellularized skeletal muscle ECM implants (DSM-ECM) (64). Additionally, the observation that this biomaterial actively functions as a macrophage and immunocell sink trap indicates an alternative application in promoting immunoresponse to ultimately stimulate tissue repair or counteract infectious disease. Neverthless, the use of nude mice or mice with immunodeficient background should be taken into account for the purpose of grafting experiments using biomaterials embedded with cells, taking under account that experimental approach could lead to bias. For example, Ma et al. used a porous collagen scaffold seeded with murine myoblasts for the treatment of skeletal muscle defects, and reported that although vascularization, innervation, and the generation of myofibers were observed, successful integration of the scaffold-tissue graft was only evident in immune-compromised animals (65).

Contrary to acellular decellularized scaffolds, that show the capability to support muscle cells infiltration (66,67) in our grafting experiments we observed that the biomaterial alone did not

recruit satellite cells on its surface thus future work will be aimed at assessing of the impact of gelatin-GP biomaterial embedded with myogenic cells. A literature study suggested the use of pre-differentiated myotubes instead of undifferentiated satellite cells, since they elicit an increased invasion of host vessels in avascular muscle bundles after 14 days from implantation in dorsal skin (68). Additionally, the observation that the biomaterial favors C2C12 cell proliferation does not exclude that the biomaterial may allow the proliferation of other types of cells and may be eventually used to deliver satellite cells (30). In our case, the long lasting of the implanted structure in TA muscle and the maintenance of its topology during time do not exclude the possibility to use this material for supporting unidirectional aligned myotubes for *in vivo* muscle engineering applications. Yang and colleagues, for example, showed that the transplantation of differentiated primary muscle cells onto biodegrable gelatin-coated nanopatterned PLGA substrate integrated in the host musculatur and led to the formation of a significantly higher number of dystrophin-positive muscle fibers compared to unpatterned patches in a model of *mdx* mice (69). Despite it may be hypothized that a better myogenesis may achieved by the use of micropatterned biomaterials also in the context of VML, this system would not be able to fill big structural voids, contrary to the recent use of acellular decellularized matrix (70,71) and hybrid PEG-fibrinogen hydrogel embedding myogenic cells (72). Despite this, contrary to our 2D system, decellularized ECM materials do not appear to achieve complete allignment between healthy and regenerating tissue, and inside 3D hydrogel cells are randomly distribuited and uniform cell allinment is generated only if sensing the tension generated by the host tissue. Anyway, the analysis of the combinatory effects of patterned biomaterial and cells, in terms of myogenic response, degradation profile and macrophages recruitment, are intriguing aspects that remain to be investigated in the contest of our scaffold. Additionally, similarly to other natural hydrogels, one advantage of gelatin-GP biomaterial is represented by the feasibility to finely tune its properties (20), so far future modifications of the micro-patterned gelatin-GP biomaterial may include the presentation or local delivery of growth factors such as IGF-1 and VEGF (57,73,74), or the modulation of the inflammatory response

focused to control the polarization of macrophages toward the M2 phenotype (75–77). For example, Wang and colleagues showed that the injection of combination of shape memory alginate gel, with embedded myogenic cells and growth factors (IGF-1 and VEGF), did not only increase the regeneration outcome after cardiotoxin damage, but also reduced the fibrotic tissue compared to the injury alone or the injection of cells and factors without scaffold (57). Despite they did not show the feasibility of this approach in VML, our biomaterial might offer the same possibility with the additional advantage to drive the orientation of cells. Therefore, the addition of selected growth factors will be considered for the future implementation of this gelatin-GP biomaterial both for *in vitro* and *in vivo* applications.

Altogether, these results provide the first characterization for the novel use of gelatin-GP biomaterial for *in vitro* and *in vivo* applications in the field of skeletal muscle tissue engineering.

Acknowledgments and Funding

This work was supported by Telethon Foundation (Grants GGP10225 and GGP14202) and the Italian Ministry of University and Research (FIRB Accordo di Programma RBAP11Z3YA_003) to P.B.; the Italian Ministry of Health (GR-2011-02346964) and the Italian Cystic Fibrosis Foundation (FFC # 20/2015) to A.R. P.P. is grateful to Camilla degli Scrovegni for continuous support and to the Italian Association for Cancer Research (AIRC, IG-14442), Telethon (GGP11139B), Italian Cystic Fibrosis Foundation (FFC #19/2014), the Italian Ministry of Education, University and Research (COFIN: 20129JLHSY_002, FIRB: RBAP11FXBC_002, Futuro in Ricerca: RBFR10EGVP_001) and the Italian Ministry of Health.

Author Disclosure Statement

The authors declare no potential conflicts of interest. No competing financial interests exist.

References

1. Zammit PS, Relaix F, Nagata Y, Ruiz AP, Collins C a, Partridge T a, et al. Pax7 and myogenic progression in skeletal muscle satellite cells. J. Cell Sci. **119**(Pt 9), 1824, 2006;

2. Qazi TH, Mooney DJ, Pumberger M, Geißler S, Duda GN. Biomaterials based strategies for skeletal muscle tissue engineering: Existing technologies and future trends. Biomaterials. Elsevier Ltd; **53**, 502, 2015;

3. Sung JH, Shuler ML. Microtechnology for mimicking in vivo tissue environment. Ann. Biomed. Eng. **40**(6), 1289, 2012;

4. Rossi CA, Pozzobon M, Coppi P De. Advances in musculoskeletal tissue engineering Moving towards therapy. **6**(3), 167, 2010;

5. Huang NF, Patel S, Thakar RG, Wu J, Hsiao BS, Chu B, et al. Myotube assembly on nanofibrous and micropatterned polymers. Nano Lett. **6**(3), 537, 2006;

6. Yamamoto DL, Csikasz RI, Li Y, Sharma G, Hjort K, Karlsson R, et al. Myotube formation on micro-patterned glass: intracellular organization and protein distribution in C2C12 skeletal muscle cells. J. Histochem. Cytochem. **56**(10), 881, 2008;

7. Sun Y, Duffy R, Lee A, Feinberg a W. Optimizing the structure and contractility of engineered skeletal muscle thin films. Acta Biomater. Acta Materialia Inc.; **9**(8), 7885, 2013;

8. Aubin H, Nichol JW, Hutson CB, Bae H, Sieminski AL, Cropek DM, et al. Directed 3D cell alignment and elongation in microengineered hydrogels. Biomaterials. **31**(27), 6941, 2010;

9. Zatti S, Zoso A, Serena E, Luni C, Cimetta E, Elvassore N. Micropatterning topology on soft substrates affects myoblast proliferation and differentiation. Langmuir. **28**(5), 2718, 2012;

10. Shah R, Knowles JC, Hunt NP, Lewis MP. Development of a novel smart scaffold for human skeletal muscle regeneration. J. Tissue Eng. Regen. Med. 2013;

11. Player DJ, Martin NRW, Passey SL, Sharples AP, Mudera V, Lewis MP. Acute mechanical overload increases IGF-I and MMP-9 mRNA in 3D tissue-engineered skeletal muscle. Biotechnol. Lett. **36**, 1113, 2014;

12. Ito A, Yamamoto Y, Sato M, Ikeda K, Yamamoto M, Fujita H, et al. Induction of functional tissue-engineered skeletal muscle constructs by defined electrical stimulation. Sci. Rep. **4**, 4781, 2014;

13. Heher P, Maleiner B, Prüller J, Teuschl AH, Kollmitzer J, Monforte X, et al. A novel bioreactor for the generation of highly aligned 3D skeletal muscle-like constructs through orientation of fibrin via application of static strain. Acta Biomater. **24**, 251, 2015;

14. Tseng TH, Chu CY, Huang JM, Shiow SJ, Wang CJ. Crocetin protects against oxidative damage in rat primary hepatocytes. Cancer Lett. **97**, 61, 1995;

15. Sung H. In vitro surface characterization of a biological patch fixed with a naturally occurring crosslinking agent. Biomaterials. **21**(13), 1353, 2000;

16. Koo HJ, Lim KH, Jung HJ, Park EH. Anti-inflammatory evaluation of gardenia extract, geniposide and genipin. J. Ethnopharmacol. **103**, 496, 2006;

17. Bigi A, Cojazzi G, Panzavolta S, Roveri N, Rubini K. Stabilization of gelatin films by crosslinking with genipin. Biomaterials. **23**, 4827, 2002;

18. Montemurro F, De Maria C, Orsi G, Ghezzi L, Tinè MR, Vozzi G. Genipin diffusion and reaction into a gelatin matrix for tissue engineering applications. J. Biomed. Mater. Res. Part B Appl. Biomater. 2015;

19. Liang H, Chang W, Lin K, Sung H. Genipin-crosslinked gelatin microspheres as a drug carrier for intramuscular administration: in vitro and in vivo studies. J. Biomed. Mater. Res. A. **65**(2), 271, 2003;

20. Solorio L, Zwolinski C, Lund AW, Farrell MJ, Stegemann JP. Gelatin microspheres

crosslinked with genipin for local delivery of growth factors. J. Tissue Eng. Regen. Med. **4**(7), 514, 2010;

21. Chang W-H, Chang Y, Lai P-H, Sung H-W. A genipin-crosslinked gelatin membrane as wound-dressing material: in vitro and in vivo studies. J. Biomater. Sci. Polym. Ed. **14**, 481, 2003;

22. Focaroli S, Teti G, Salvatore V, Durante S, Belmonte MM, Giardino R, et al. Chondrogenic differentiation of human adipose mesenchimal stem cells: Influence of a biomimetic gelatin genipin crosslinked porous scaffold. Microsc. Res. Tech. **77**(11), 928, 2014;

23. Chen Y-S, Chang J-Y, Cheng C-Y, Tsai F-J, Yao C-H, Liu B-S. An in vivo evaluation of a biodegradable genipin-cross-linked gelatin peripheral nerve guide conduit material. Biomaterials. **26**(18), 3911, 2005;

24. Chang J-Y, Ho T-Y, Lee H-C, Lai Y-L, Lu M-C, Yao C-H, et al. Highly permeable genipin-cross-linked gelatin conduits enhance peripheral nerve regeneration. Artif. Organs. **33**(12), 1075, 2009;

25. Lien SM, Li WT, Huang TJ. Genipin-crosslinked gelatin scaffolds for articular cartilage tissue engineering with a novel crosslinking method. Mater. Sci. Eng. C. **28**, 36, 2008;

26. Vozzi G, Corallo C, Carta S, Fortina M, Gattazzo F, Galletti M, et al. Collagen-gelatin-genipin-hydroxyapatite composite scaffolds colonized by human primary osteoblasts are suitable for bone tissue engineering applications: in vitro evidences. J. Biomed. Mater. Res. A. **102**(5), 1415, 2014;

27. Sharifi E, Azami M, Kajbafzadeh A-M, Moztarzadeh F, Faridi-Majidi R, Shamousi A, et al. Preparation of a biomimetic composite scaffold from gelatin/collagen and bioactive glass fibers for bone tissue engineering. Mater. Sci. Eng. C. Mater. Biol. Appl. **59**, 533, 2016;

28. Carrabba M, Maria C De, Oikawa A, Reni C, Rodriguez-Arabaolaza I, Spencer H, et al.

Design, fabrication and perivascular implantation of bioactive scaffolds engineered with human adventitial progenitor cells for stimulation of arteriogenesis in peripheral ischemia. Biofabrication. **8**(1), 15020, 2016;

29. Boldrin L, Elvassore N, Malerba A, Flaibani M, Cimetta E, Piccoli M, et al. Satellite cells delivered by micro-patterned scaffolds: a new strategy for cell transplantation in muscle diseases. Tissue Eng. **13**(2), 253, 2007;

30. Rossi CA, Flaibani M, Blaauw B, Pozzobon M, Figallo E, Reggiani C, et al. In vivo tissue engineering of functional skeletal muscle by freshly isolated satellite cells embedded in a photopolymerizable hydrogel. FASEB J. **25**(7), 2296, 2011;

31. Gattazzo F, Molon S, Morbidoni V, Braghetta P, Blaauw B, Urciuolo A, et al. Cyclosporin A Promotes in vivo Myogenic Response in Collagen VI-Deficient Myopathic Mice. Front. Aging Neurosci. **6**(September), 244, 2014;

32. Engler AJ, Griffin MA, Sen S, Bönnemann CG, Sweeney HL, Discher DE. Myotubes differentiate optimally on substrates with tissue-like stiffness: Pathological implications for soft or stiff microenvironments. J. Cell Biol. **166**, 877, 2004;

33. Gilbert PM, Havenstrite KL, Magnusson KEG, Sacco A, Leonardi NA, Kraft P, et al. Substrate elasticity regulates skeletal muscle stem cell self-renewal in culture. Science. **329**(5995), 1078, 2010;

34. Charest JL, García AJ, King WP. Myoblast alignment and differentiation on cell culture substrates with microscale topography and model chemistries. Biomaterials. **28**, 2202, 2007;

35. Bajaj P, Reddy B, Millet L, Wei C, Zorlutuna P, Bao G, et al. Patterning the differentiation of C2C12 skeletal myoblasts. Integr. Biol. (Camb). **3**(9), 897, 2011;

36. Shen C-C, Yang Y-C, Liu B-S. Peripheral nerve repair of transplanted undifferentiated adipose tissue-derived stem cells in a biodegradable reinforced nerve conduit. J. Biomed.

Mater. Res. A. **100**(1), 48, 2012;

37. Engler AJ, Sen S, Sweeney HL, Discher DE. Matrix elasticity directs stem cell lineage specification. Cell. **126**(4), 677, 2006;

38. Humphrey JD, Dufresne ER, Schwartz MA. Mechanotransduction and extracellular matrix homeostasis. Nat. Publ. Gr. Nature Publishing Group; **15**(12), 802, 2014;

39. Collinsworth AM, Zhang S, Kraus WE, Truskey G a. Apparent elastic modulus and hysteresis of skeletal muscle cells throughout differentiation. AJP Cell Physiol. **283**(4), C1219, 2002;

40. Boontheekul T, Hill EE, Kong H-J, Mooney DJ. Regulating myoblast phenotype through controlled gel stiffness and degradation. Tissue Eng. **13**(7), 1431, 2007;

41. Jun I, Jeong S, Shin H. The stimulation of myoblast differentiation by electrically conductive sub-micron fibers. Biomaterials. **30**(11), 2038, 2009;

42. Shimizu K, Fujita H, Nagamori E. Alignment of skeletal muscle myoblasts and myotubes using linear micropatterned surfaces ground with abrasives. Biotechnol. Bioeng. **103**(3), 631, 2009;

43. Huang NF, Lee RJ, Li S. Engineering of aligned skeletal muscle by micropatterning. Am. J. Transl. Res. **2**(1), 43, 2010;

44. Serena E, Zatti S, Reghelin E, Pasut A, Cimetta E, Elvassore N. Soft substrates drive optimal differentiation of human healthy and dystrophic myotubes. Integr. Biol. (Camb). **2**(4), 193, 2010;

45. Ku SH, Lee SH, Park CB. Synergic effects of nanofiber alignment and electroactivity on myoblast differentiation. Biomaterials. **33**(26), 6098, 2012;

46. Hosseini V, Ahadian S, Ostrovidov S, Camci-Unal G, Chen S, Kaji H, et al. Engineered Contractile Skeletal Muscle Tissue on a Microgrooved Methacrylated Gelatin Substrate.

Tissue Eng. Part A. **18**(23-24), 2453, 2012;

47. Monge C, Ren K, Berton K, Guillot R, Peyrade D, Picart C. Engineering Muscle Tissues on Microstructured Polyelectrolyte Multilayer Films. Tissue Eng. Part A. **18**, 1664, 2012;

48. Sengupta D, Gilbert PM, Johnson KJ, Blau HM, Heilshorn SC. Protein-Engineered Biomaterials to Generate Human Skeletal Muscle Mimics. Adv. Healthc. Mater. **1**(6), 785, 2012;

49. Teixeira AI, Abrams G a, Bertics PJ, Murphy CJ, Nealey PF. Epithelial contact guidance on well-defined micro- and nanostructured substrates. J. Cell Sci. **116**, 1881, 2003;

50. Vogel V, Sheetz M. Local force and geometry sensing regulate cell functions. Nat. Rev. Mol. Cell Biol. **7**, 265, 2006;

51. Kim DH, Han K, Gupta K, Kwon KW, Suh KY, Levchenko A. Mechanosensitivity of fibroblast cell shape and movement to anisotropic substratum topography gradients. Biomaterials. Elsevier Ltd; **30**(29), 5433, 2009;

52. Shimizu K, Fujita H, Nagamori E. Micropatterning of single myotubes on a thermoresponsive culture surface using elastic stencil membranes for single-cell analysis. J. Biosci. Bioeng. The Society for Biotechnology, Japan; **109**(2), 174, 2010;

53. Chen M-C, Sun Y-C, Chen Y-H. Electrically conductive nanofibers with highly oriented structures and their potential application in skeletal muscle tissue engineering. Acta Biomater. [Internet]. Acta Materialia Inc.; **9**(3), 5562, 2013 [cited 2015 Jan 1]; Available from: http://www.ncbi.nlm.nih.gov/pubmed/23099301

54. Bettadapur A, Suh GC, Geisse NA, Wang ER, Hua C, Huber HA, et al. Prolonged Culture of Aligned Skeletal Myotubes on Micromolded Gelatin Hydrogels. Sci. Rep. Nature Publishing Group; **6**, 28855, 2016;

55. Hwang YJ, Larsen J, Krasieva TB, Lyubovitsky JG. Effect of genipin crosslinking on the

optical spectral properties and structures of collagen hydrogels. ACS Appl. Mater. Interfaces. **3**(7), 2579, 2011;

56. Gates C, Huard J. Management of skeletal muscle injuries in military personnel. Oper. Tech. Sports Med. **13**, 247, 2005;

57. Wang L, Cao L, Shansky J, Wang Z, Mooney D, Vandenburgh H. Minimally invasive approach to the repair of injured skeletal muscle with a shape-memory scaffold. Mol. Ther. **22**(8), 1441, 2014;

58. Perniconi B, Costa A, Aulino P, Teodori L, Adamo S, Coletti D. The pro-myogenic environment provided by whole organ scale acellular scaffolds from skeletal muscle. Biomaterials [Internet]. Elsevier Ltd; **32**(31), 7870, 2011 [cited 2014 Dec 18]; Available from: http://www.ncbi.nlm.nih.gov/pubmed/21802724

59. Hurd S a., Bhatti NM, Walker AM, Kasukonis BM, Wolchok JC. Development of a biological scaffold engineered using the extracellular matrix secreted by skeletal muscle cells. Biomaterials [Internet]. Elsevier Ltd; **49**, 9, 2015; Available from: http://linkinghub.elsevier.com/retrieve/pii/S0142961215000447

60. Wang L, Shansky J, Borselli C, Mooney D, Vandenburgh H. Design and Fabrication of a Biodegradable, Covalently Crosslinked Shape-Memory Alginate Scaffold for Cell and Growth Factor Delivery. Tissue Eng. Part A. **18**, 2000, 2012;

61. Anderson JM, Rodriguez A, Chang DT. Foreign body reaction to biomaterials. Semin. Immunol. **20**(2), 86, 2008;

62. Tidball JG, Villalta SA. Regulatory interactions between muscle and the immune system during muscle regeneration. Am. J. Physiol. Regul. Integr. Comp. Physiol. **298**(5), R1173, 2010;

63. Mantovani A, Biswas SK, Galdiero MR, Sica A, Locati M. Macrophage plasticity and

polarization in tissue repair and remodelling. J. Pathol. **229**(2), 176, 2013;

64. Fishman JM, Lowdell MW, Urbani L, Ansari T, Burns AJ, Turmaine M, et al. Immunomodulatory effect of a decellularized skeletal muscle scaffold in a discordant xenotransplantation model. Proc. Natl. Acad. Sci. U. S. A. **110**(35), 14360, 2013;

65. Ma J, Holden K, Zhu J, Pan H, Li Y. The application of three-dimensional collagen-scaffolds seeded with myoblasts to repair skeletal muscle defects. J. Biomed. Biotechnol. [Internet]. **2011**, 812135, 2011 [cited 2015 Jan 1]; Available from: http://www.pubmedcentral.nih.gov/articlerender.fcgi?artid=3238809&tool=pmcentrez&rendertype=abstract

66. Mase VJ, Hsu JR, Wolf SE, Wenke JC, Baer DG, Owens J, et al. Clinical application of an acellular biologic scaffold for surgical repair of a large, traumatic quadriceps femoris muscle defect. Orthopedics. **33**, 511, 2010;

67. DeQuach JA, Lin JE, Cam C, Hu D, Salvatore MA, Sheikh F, et al. Injectable skeletal muscle matrix hydrogel promotes neovascularization and muscle cell infiltration in a hindlimb ischemia model. Eur. Cells Mater. **23**, 400, 2012;

68. Juhas M, Engelmayr GC, Fontanella AN, Palmer GM, Bursac N. Biomimetic engineered muscle with capacity for vascular integration and functional maturation in vivo. Proc. Natl. Acad. Sci. U. S. A. 2014;

69. Yang HS, Ieronimakis N, Tsui JH, Kim HN, Suh KY, Reyes M, et al. Nanopatterned muscle cell patches for enhanced myogenesis and dystrophin expression in a mouse model of muscular dystrophy. Biomaterials. Elsevier Ltd; **35**(5), 1478, 2014;

70. Sicari BM, Rubin JP, Dearth CL, Wolf MT, Ambrosio F, Boninger M, et al. An acellular biologic scaffold promotes skeletal muscle formation in mice and humans with volumetric muscle loss. Sci. Transl. Med. **6**(234), 234ra58, 2014;

71. Corona BT, Ward CL, Baker HB, Walters TJ, Christ GJ. Implantation of in vitro tissue engineered muscle repair constructs and bladder acellular matrices partially restore in vivo skeletal muscle function in a rat model of volumetric muscle loss injury. Tissue Eng. Part A. **20**(3-4), 705, 2014;

72. Fuoco C, Rizzi R, Biondo A, Longa E, Mascaro A, Shapira-Schweitzer K, et al. In vivo generation of a mature and functional artificial skeletal muscle. EMBO Mol. Med. **7**(4), 411, 2015;

73. Yang HS, Ieronimakis N, Tsui JH, Kim HN, Suh KY, Reyes M, et al. Nanopatterned muscle cell patches for enhanced myogenesis and dystrophin expression in a mouse model of muscular dystrophy. Biomaterials. **35**(5), 1478, 2014;

74. Borselli C, Storrie H, Benesch-Lee F, Shvartsman D, Cezar C, Lichtman JW, et al. Functional muscle regeneration with combined delivery of angiogenesis and myogenesis factors. Proc. Natl. Acad. Sci. **107**(8), 3287, 2010;

75. Vasconcelos DP, Costa M, Amaral IF, Barbosa MA, Águas AP, Barbosa JN. Development of an immunomodulatory biomaterial: using resolvin D1 to modulate inflammation. Biomaterials. **53**, 566, 2015;

76. Alvarez MM, Liu JC, Trujillo-de Santiago G, Cha B-H, Vishwakarma A, Ghaemmaghami AM, et al. Delivery strategies to control inflammatory response: Modulating M1-M2 polarization in tissue engineering applications. J. Control. Release. 2016;

77. Emeterio CLS, Olingy CE, Chu Y, Botchwey EA. Biomaterials Selective recruitment of non-classical monocytes promotes skeletal muscle repair. Biomaterials [Internet]. Elsevier Ltd; **117**, 32, 2017; Available from: http://dx.doi.org/10.1016/j.biomaterials.2016.11.021

Figure legends

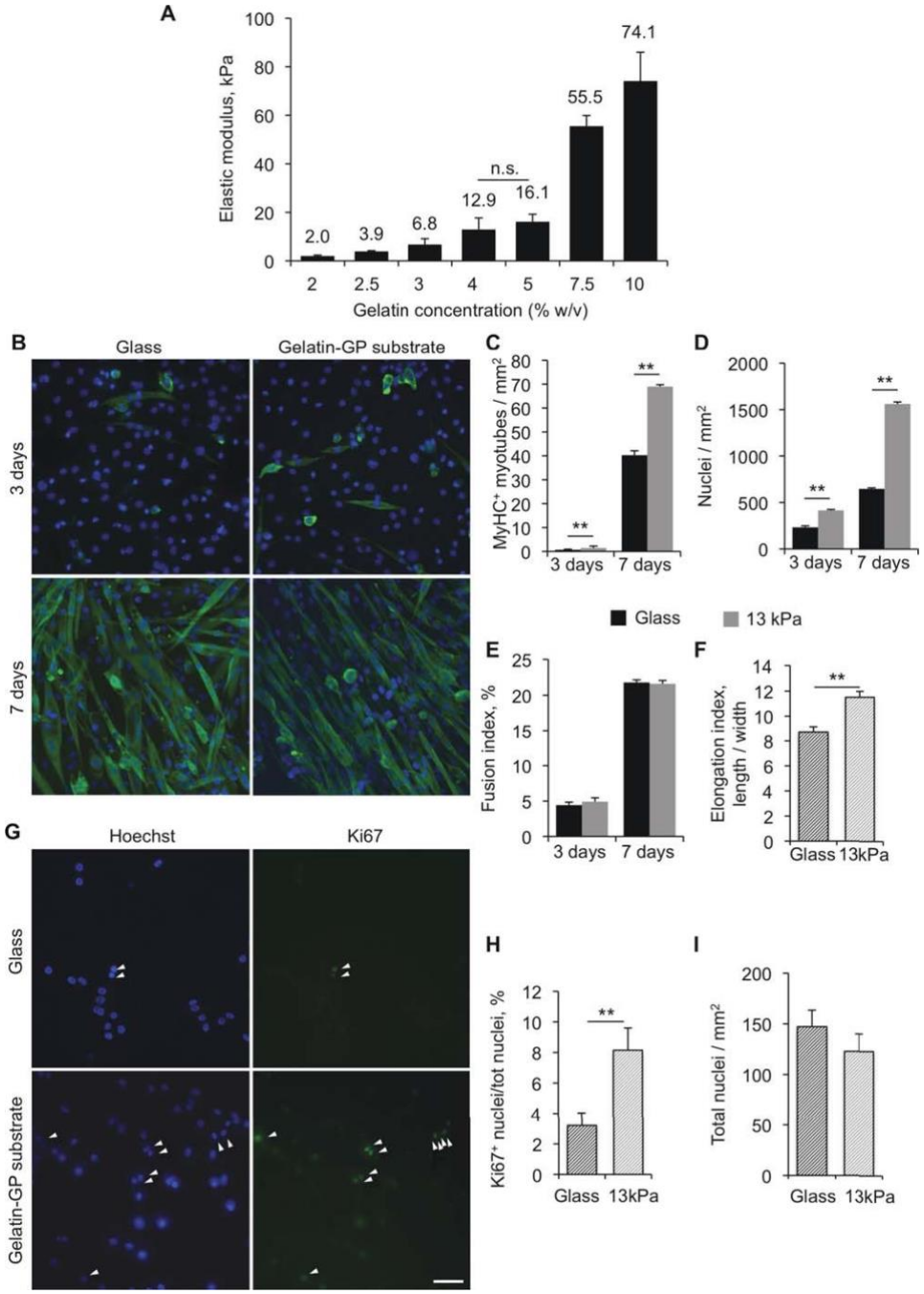

Figure 1. Gelatin-GP substrates sustain myoblast growth and differentiation. A. Quantification of the compressive elastic modulus of biomimetic structures composed of gelatin cross-linked with 0.2% GP, as function of increasing concentrations of gelatin (given as % w/v in PBS). Data represent the mean ± s.d. of three independent replicates (unequal variance Student's t test; $n = 10$ structures, each group; n.s. not significant. $P < 0.05$ where not indicated). **B.** Immunofluorescence

719 staining for MyHC (green) in C2C12 myotubes differentiated for 3 days or 7 days on glass or on 13
720 kPa gelatin-GP substrates. Nuclei were stained with Hoechst (blue). Scale bar, 50 μm. **C-E**.
721 Morphological parameters evaluated on C2C12 myotubes grown for 3 days or 7 days on glass or on
722 13 kPa gelatin-GP substrates, and corresponding to the quantification of the total number of
723 myotubes per area unit (**C**), the total number of nuclei per area unit (**D**) and the fusion index
724 calculated as the percentage of nuclei inside myotubes on total nuclei (**E**). Error bars indicate s.e.m.
725 (**, $P < 0.01$; $n = 3$). **F.** Quantification of elongation index, calculated the as ratio between myotube
726 length and myotube width. Error bars indicate s.e.m. (**, $P < 0.01$; $n = 3$). **G.** Immunofluorescence
727 staining for Ki67 (green) on C2C12 cell cultures grown for 24 hr on glass or on 13 kPa gelatin-GP
728 substrates. Nuclei were stained with Hoechst (blue). Scale bar, 50 μm. **H.** Percentage of
729 proliferating C2C12 cells grown on glass or on 13 kPa gelatin-GP substrates, calculated as Ki67-
730 positive nuclei on total nuclei. Error bars indicate s.e.m. (**, $P < 0.01$; $n = 3$). **I.** Quantification of
731 the total number of nuclei per area unit of C2C12 cells grown on glass or on 13 kPa gelatin-GP
732 substrates. Data are expressed as mean ± s.e.m. (not significant; $n = 3$).
733

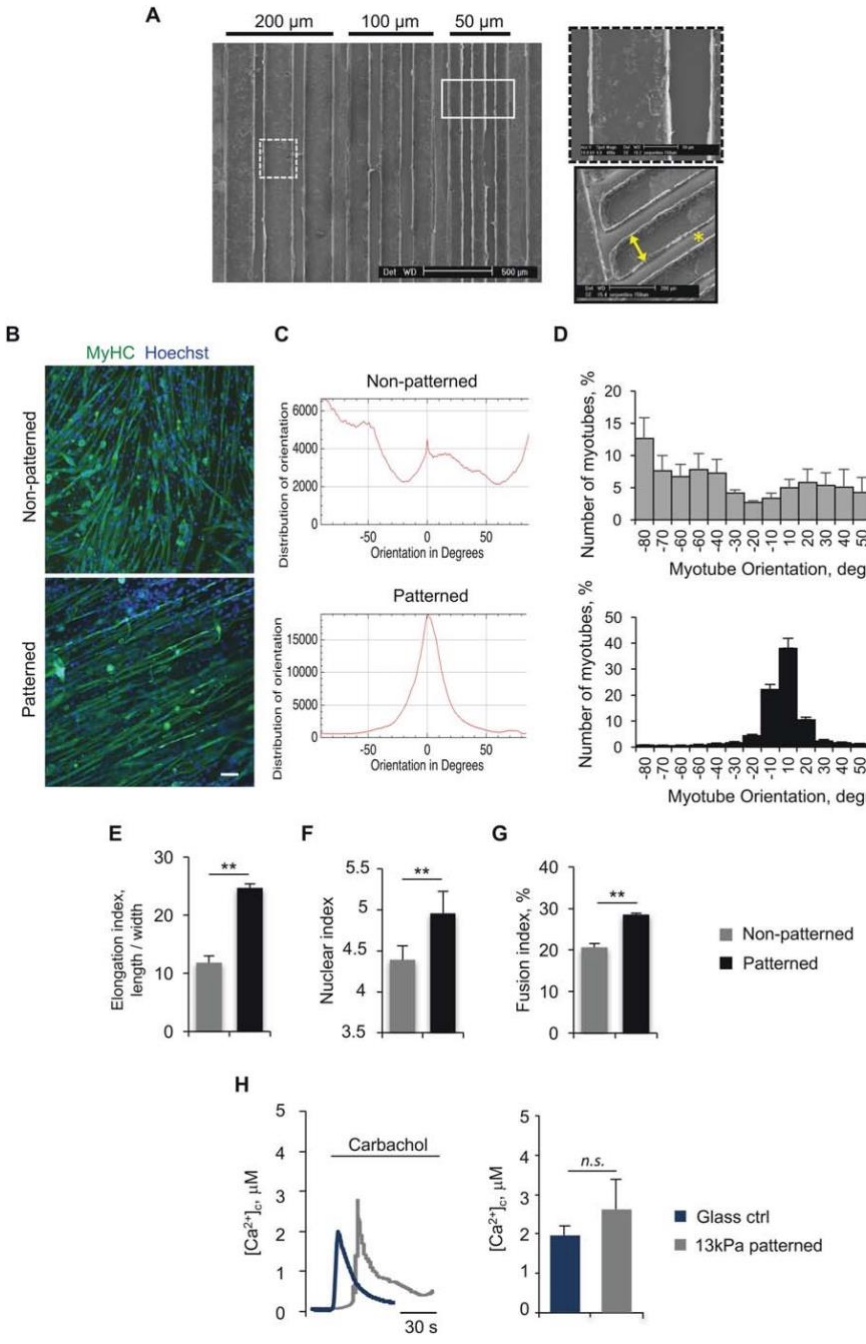

Figure 2. Micro-patterned gelatin-GP substrates promote the alignment, elongation and fusion of myoblasts. A. Scanning electron microscope analysis of dry graded aligned structures. The aligned strips are 200, 100 and 50 µm wide, 40 µm high and 100 µm apart. Higher magnifications of frontal view (upper panel) and lateral view (lower panel) are shown on the right.

741 Arrowed line indicates the width of channel separation, asterisk highlights the 40 μm high channel.
742 **B.** Immunofluorescence staining for MyHC (green) in C2C12 myotubes differentiated for 7 days on
743 non-patterned or micro-patterned gelatin-GP substrates with a stiffness of 13 kPa. Nuclei were
744 stained with Hoechst (blue). Scale bars, 75 μm. **C-F.** Quantification of morphological parameters of
745 C2C12 myotubes differentiated for 7 days on non-patterned and micro-patterned gelatin-GP
746 substrates, and corresponding to: percentage of aligned myotubes, calculated as the number of
747 myotubes with an orientation degree lower than 10° with respect to the main direction of the micro-
748 patterning, on the total number of myotubes (**C**); elongation index, calculated as the ratio between
749 myotube length and myotube width (**D**); nuclear index, calculated as the mean number of nuclei
750 inside myotubes (**E**); fusion index, calculated as the percentage of nuclei inside myotubes on total
751 nuclei (**F**). Data are expressed as mean± s.e.m. (**, $P < 0.01$; $n = 5$). **G.** Analysis of calcium fluxes
752 with Fura-2/AM after carbachol stimulation of C2C12 myotubes differentiated for 7 days on micro-
753 patterned 13 kPa gelatin-GP substrates. The left panel shows the cytosolic calcium concentrations
754 ($[Ca^{2+}]_c$) at different times after carbachol stimulation, the right panel is an histogram of the peak
755 calcium levels of different myotubes. Error bars indicate s.e.m. ($n = 5$).
756

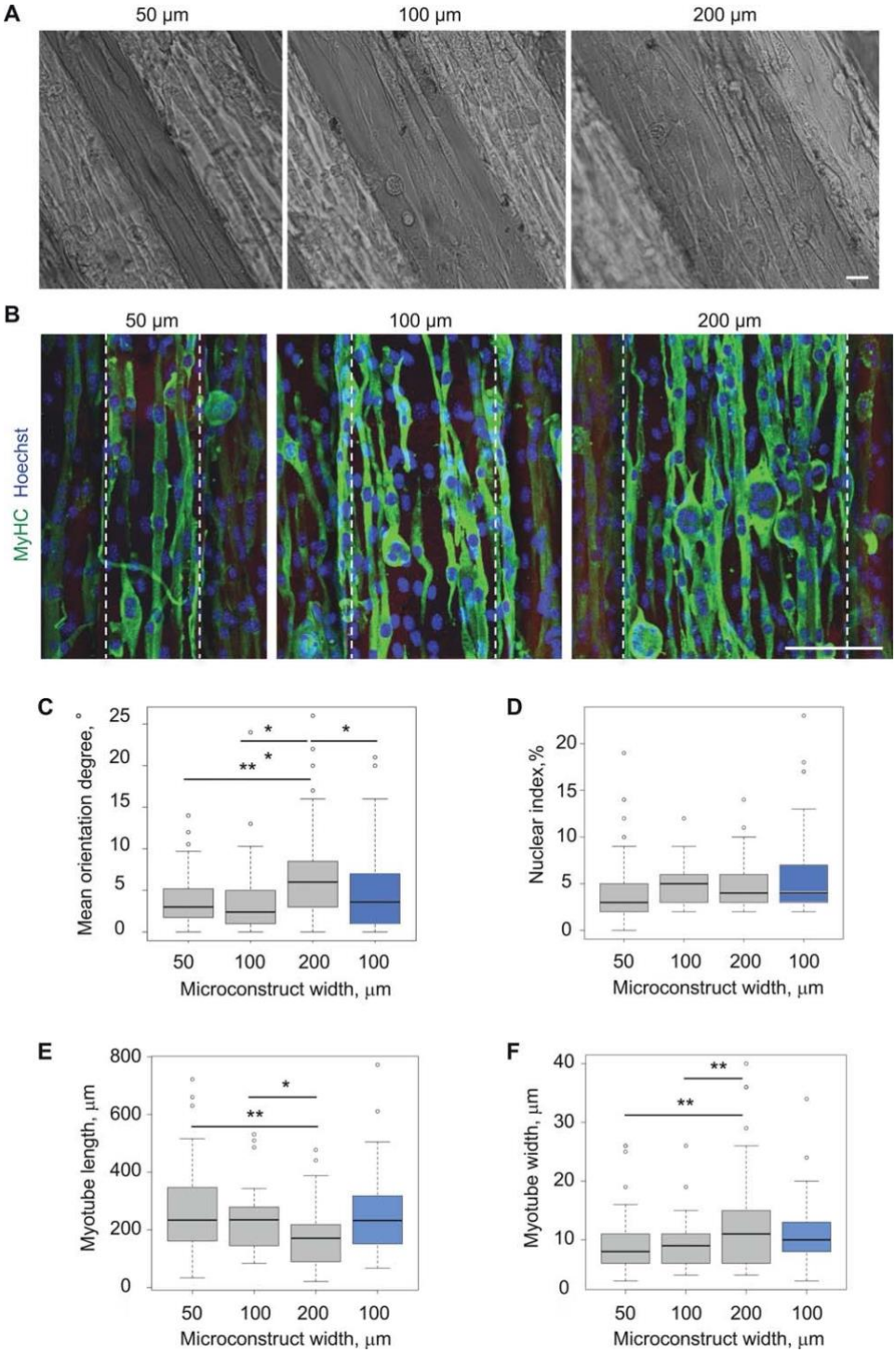

Figure 3. Strip spacing of micro-patterned gelatin-GP structures influences C2C12 myotubes.

A. Representative light microscopy images of C2C12 myoblasts cultured in differentiation medium for 7 days onto 12 kPa gelatin-GP micro-patterned structures with 50 µm, 100 µm or 200 µm wide

763 strips. Scale bar, 75 μm. **B.** Immunofluorescence staining for MyHC (green) on C2C12
764 differentiated for 7 days onto 13 kPa micro-patterned GP-gelatin biomaterial with 50 μm, 100 μm
765 or 200 μm wide strips. Nuclei were stained with Hoechst (blue). Scale bar, 100 μm. **C.** Mean
766 orientation degree of C2C12 myotubes grown on 50 μm, 100 μm or 200 μm wide strips (black) and
767 100 μm groove (light blue). Error bars indicate s.e.m. (**, $P < 0.01$; **, $P < 0.05$; $n = 3$). **D.**
768 Quantification of the nuclear index of C2C12 myotubes cultured on 50 μm, 100 μm or 200 μm
769 wide strips (black) and 100 μm groove (light blue). Error bars indicate s.e.m. (not significant; $n =$
770 3). **E, F.** Quantification of the average length (**E**) and of the average width (**F**) of C2C12 myotubes
771 cultured on 50 μm, 100 μm or 200 μm wide strips (black) and 100 μm groove (light blue). Error
772 bars indicate s.d. (*, $P < 0.05$; **, $P < 0.03$; $n = 3$). At least 300 myotubes were considered for each
773 condition.

774

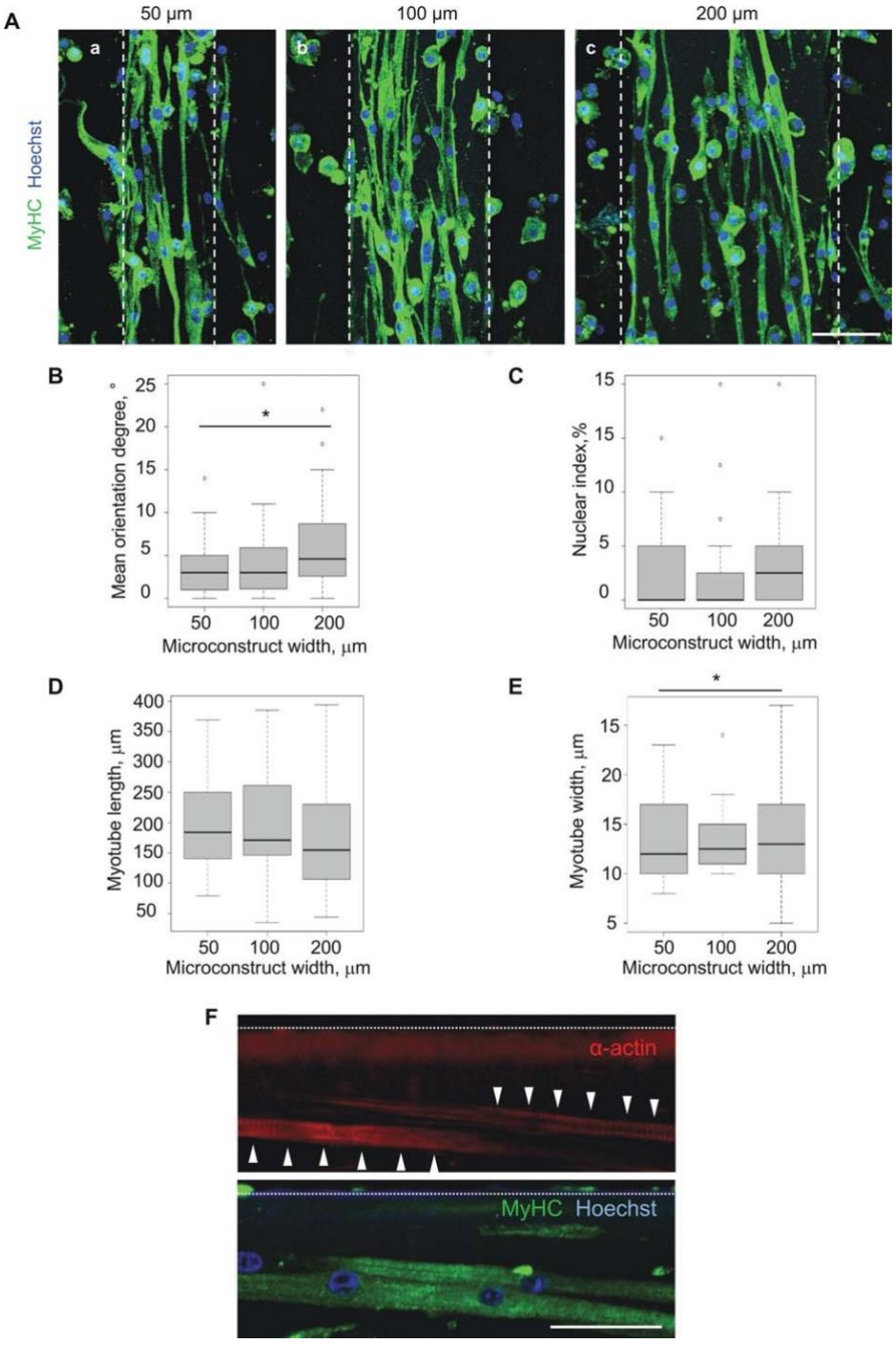

Figure 4. Micro-patterned gelatin-GP biomaterials guide the orientation of primary myotubes. A. Immunofluorescence staining for MyHC (green) of primary mouse myotubes cultured for 7 days onto 13 kPa micro-patterned GP-gelatin structures with 50 µm, 100 µm or 200

μm wide strips. Nuclei were stained with Hoechst (blue). Scale bar, 75 μm. **B.** Mean orientation degree of primary mouse myotubes grown on 50 μm, 100 μm or 200 μm wide strips. Error bars indicate s.e.m. (*, $P < 0.05$; $n = 3$). **C.** Quantification of the nuclear index of primary mouse myotubes cultured on 50 μm, 100 μm or 200 μm wide strips. Error bars indicate s.e.m. (not significant; $n = 3$). **D, E.** Quantification of the average length (**D**) and of the average width (**E**) of primary mouse myotubes cultured on 50 μm, 100 μm or 200 μm wide strips. Error bars indicate s.d. (*, $P < 0.05$; $n = 3$). At least 100 myotubes were considered for each condition. **F.** Immunofluorescence staining for MyHC (green) and α-actin (red) of primary wild-type myotubes cultured on micro-patterned structures. The arrows point at the the formation of the contractile apparatus. The dotted line indicates strip spacing. Scale bar, 25 μm.

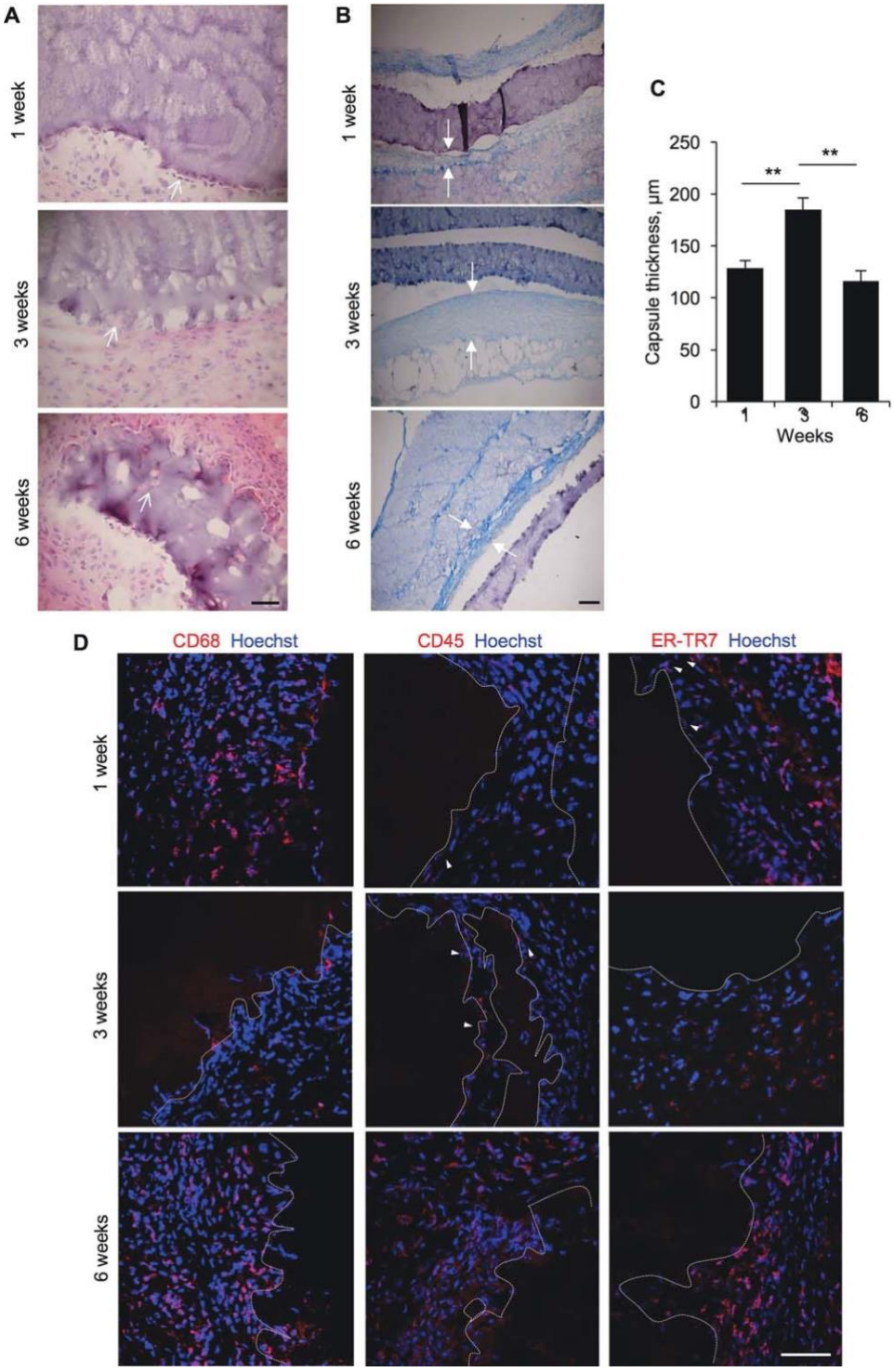

Figure 5. Analysis of subcutaneous *in vivo* grafting of micro-patterned gelatin-GP scaffolds under mouse dorsal skin. A. Hematoxylin-eosin staining of mouse back skin sections at 1 week, 3

weeks and 6 weeks after subcutaneous implantation of micro-patterned gelatin-GP biomaterial. The arrows point at some mononucleated cells adherent or infiltrating the implanted structure. Scale bar, 50 μm. **B.** Measurement of the thickness of the micro-patterned gelatin-GP at 1 week, 3 weeks and 6 weeks after subcutaneous implantation. Error bars indicate s.e.m. (**, $P < 0.03$; $n = 3$ animals, each group). C. Azan-Mallory staining of mouse back skin sections at 1 week, 3 weeks and 6 weeks after subcutaneous implantation of the micro-patterned biomaterial. The arrows mark the fibrotic tissue capsule surrounding the implant. Scale bar, 100 μm. **D.** Measurement of the thickness of the foreign body capsule at 1 week, 3 weeks and 6 weeks after subcutaneous implantation of the micro-patterned biomaterial. Error bars indicate s.e.m. (**, $P < 0.03$; $n = 3$ animals, each group). **E.** Immunofluorescence staining for CD68, CD45 and ER-TR7 (red) of subcutaneous tissue sections at 1 week, 3 weeks and 6 weeks after subcutaneous implantation of the micro-patterned biomaterial. Nuclei were stained with Hoechst (blue). The dotted black areas mark the micro-patterned scaffold. The arrowheads point at some cells adherent to the scaffold. Scale bar, 50 μm.

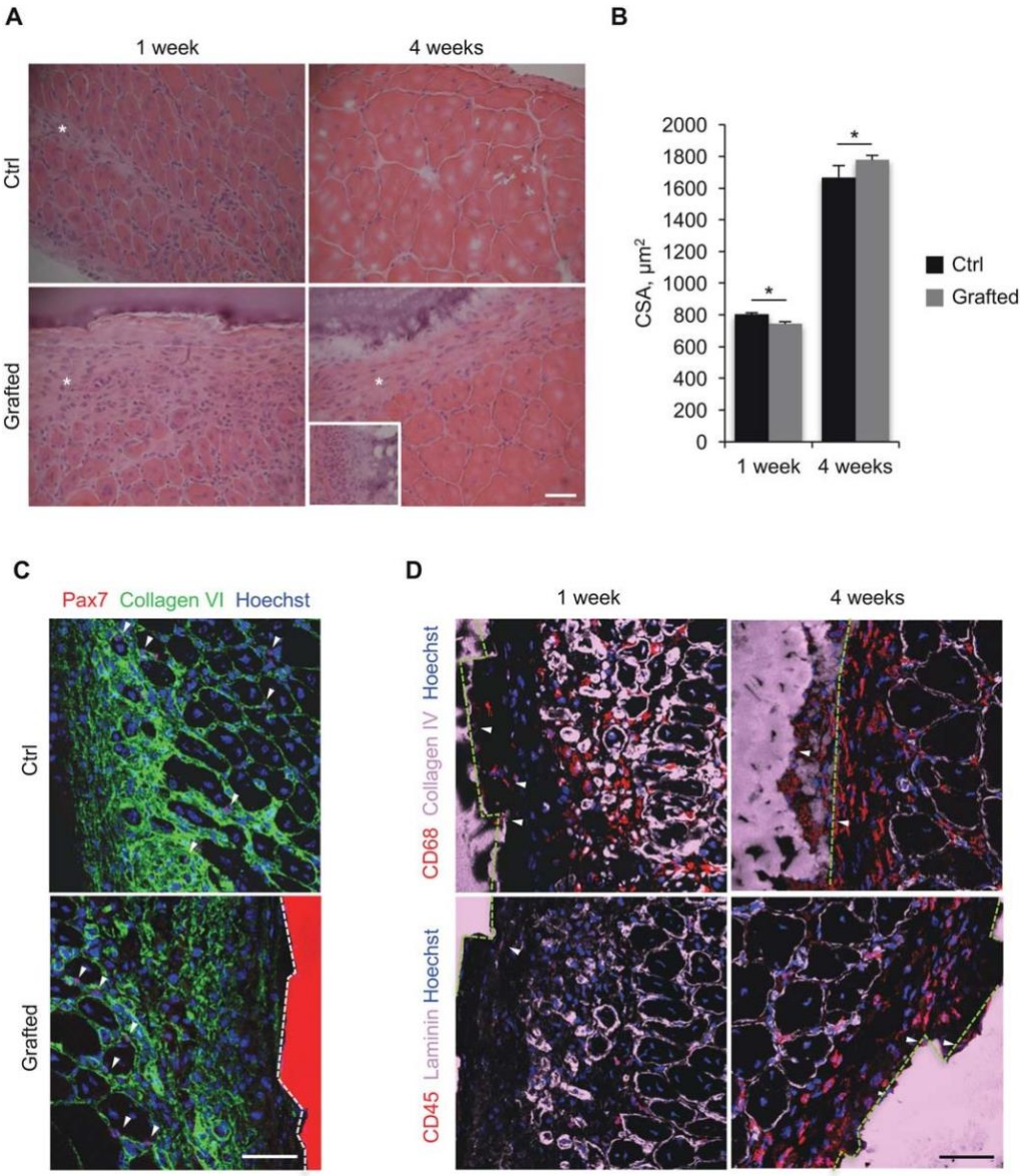

Figure 6. Analysis of injured mouse TA muscles grafted with micro-patterned gelatin-GP scaffolds. A. Hematoxylin-eosin staining of mouse TA cross-sections 1 week and 4 weeks after partial surgical muscle ablation (Ctrl) and grafting with the micro-patterned gelatin-GP biomaterial (Grafted). The asterisks mark some mononucleated cells. The inset shows mononucleated cells invading the biomaterial at the borders. Scale bar, 100 µm. **B.** Mean cross-sectional area (CSA) of centrally nucleated fibers 1 week and 4 weeks after partial surgical muscle ablation (Ctrl) and

grafting with the micro-patterned biomaterial (Grafted). Error bars indicate s.e.m. (**, $P < 0.03$; n = 3 animals, each group). **C.** Double immunofluorescence labeling for collagen VI (green) and Pax7 (red) of mouse TA cross-sections 7 days after partial surgical muscle ablation (Ctrl) and after grafting with the micro-patterned biomaterial (Grafted). Nuclei were stained with Hoechst (blue). Arrowheads point at some Pax7-positive cells. The dotted area marks the autofluorescent scaffold. Scale bar, 50 μm. **D.** Double immunofluorescence labeling for CD68 (red) and collagen IV (pink, upper panels) or laminin (pink, lower panels) of mouse TA cross-sections 1 week and 4 weeks after grafting with the micro-patterned biomaterial in the damaged region. Nuclei were stained with Hoechst (blue). Arrowheads point at some adherent cells. The dotted areas mark the autofluorescent scaffold. Scale bar, 50 μm.